Macromolecules

Article

pubs.acs.org/Macromolecules

Gas Sorption and Diffusion in Amorphous and Semicrystalline Nanoporous Poly(2,6-dimethyl-1,4-phenylene)oxide

Michele Galizia,[†,*] Christophe Daniel,[‡] Gianluca Fasano,[‡] Gaetano Guerra,[‡] and Giuseppe Mensitieri[§]

[†]Department of Materials and Production Engineering, University of Naples Federico II, p.le Tecchio 80, 80125 Naples, Italy

[‡]Department of Chemistry, NANOMATES and INSTM Research Unit, University of Salerno, via Ponte Don Melillo, 84084 Fisciano (SA), Italy

[§]Department of Materials and Production Engineering and INSTM Research Unit, University of Naples Federico II, p.le Tecchio 80, 80125 Naples, Italy

ABSTRACT: In this contribution is presented an analysis of mass transport properties of low molecular weight compounds in amorphous PPO and in two semicrystalline PPOs obtained by treating with benzene and carbon tetrachloride the amorphous sample. It is found that semicrystalline samples are endowed with larger gas sorption capacity and diffusivity as compared to the amorphous ones: this behavior has been attributed prevalently to the nanoporous nature of the crystalline phases induced by treatment with solvents. In particular, sorption experiments, carried out at 30 °C with methane, carbon dioxide, propane and propylene, have shown that both semicrystalline PPOs display rather interesting features which make them suitable for use as membrane materials in gas separation processes, in view of the relatively high values of solubility and diffusivity. Moreover, these peculiar sorption and mass transport properties have been found to be virtually unaffected by thermal aging: in fact, sorption experiments conducted on amorphous and semicrystalline PPO after treatment at 65 °C for three months showed that sorption and transport properties of aged samples are the same as for the untreated ones. This is an important feature to ensure the stability of performances in membrane applications.

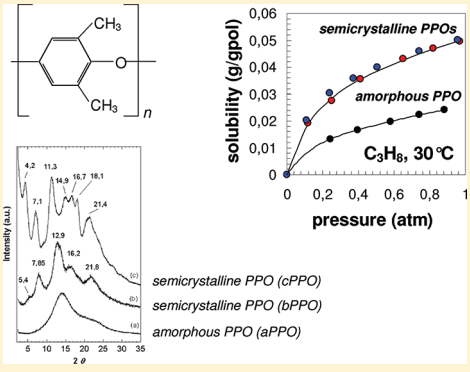

1. INTRODUCTION

Poly(2,6-dimethyl-1,4-phenylene)oxide (PPO) is an aromatic amorphous polymer (see Figure 1 for the repeating unit)

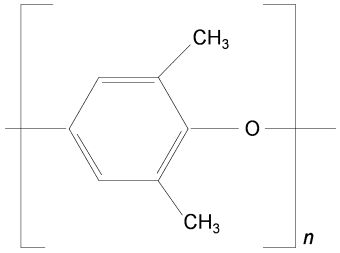

Figure 1. Repeating unit of PPO.

showing very high values of glass transition temperature and gas permeability. Previous works[1,2] report, for amorphous PPO, high levels of gas solubility, diffusivity and permeability, showing its suitability for use as a membrane for gas separations. Ideal separation factors were estimated for different penetrant couples of practical concern, such as methane/carbon dioxide and propane/propylene.[1,2] As pointed out by Toi et al.,[3] the permeation rate of PPO results several times larger than that of many other common glassy and even rubbery polymers. This finding, rather unusual in view of the very high glass transition temperature of PPO and considering the high rigidity of its molecular backbone, has been attributed to the relatively high fractional free volume, f, which was estimated to be about 18%.[4] It is recalled that f is defined as $(\hat{V}_{sp} - \hat{V}_0)/\hat{V}_{sp}$, where $\hat{V}_{sp}$ is the specific volume and $\hat{V}_0$ the occupied volume, as calculated through the Bondi's rule.

These features make PPO attractive for its exploitation as membrane material for gas separation, also in view of the fact that PPO is a commercial polymer with a cost which is well below that of common techno-polymers.

Quite interestingly, it has been found that semicrystalline PPO displaying nanoporous crystalline phases can be obtained by treatment with specific solvents.[5,6] As recently demonstrated by Guerra and co-workers,[7−14] semicrystalline PPO is characterized by peculiar and unexpected properties which resemble those of semicrystalline syndiotactic polystyrene (sPS) with nanoporous crystalline domains. In particular, it has been observed[7−15] that, in spite of the presence of a crystalline phase, the solubility of several low molecular weight compounds is significantly higher in semicrystalline PPO than in the totally amorphous PPO. In fact, this behavior has been attributed to sorption within the nanoporous crystalline phase.

Received: January 9, 2012
Revised: March 28, 2012
Published: April 13, 2012

   dx.doi.org/10.1021/ma3000626 | *Macromolecules* 2012, 45, 3604−3615

Usually, the description of gas solubility isotherms in semicrystalline polymers is based on the simple assumption that the penetrant molecules are accommodated only in the amorphous phase and that the crystalline domains do not contribute to the sorption process, because of its inaccessible and closely packed structure. Such an assumption has been widely confirmed by experimental evidence. As a consequence, the total gas solubility coefficient in the whole semicrystalline sample, S, can be generally scaled to that of the sole amorphous phase, S_a, according to the simple expression

$$S = \chi S_a \tag{1}$$

where χ is the volume fraction of amorphous phase.[16−18] The solubility coefficient is defined as the ratio between the equilibrium penetrant concentration inside the polymer (expressed as (cm^3 (STP)) /(cm^3 of polymer)) and the value of the external partial pressure of penetrant in contact with polymer. Nevertheless, in some cases this physical picture appears oversimplified, as for semicrystalline polymers displaying the mentioned nanoporous crystalline phases that contribute to sorption of low molecular weight compounds in a nonnegligible amount. One of the first reported cases is that of poly(4-methyl-1-pentene) (PMP).[19,20] Later, several authors demonstrated that, in some cases, the crystalline phase gives a contribution to the total solubility that even largely exceeds that of the amorphous phase: such a behavior was observed, for instance, in semicrystalline syndiotactic poly styrene (sPS).[8−14] In fact, in the case of carbon dioxide sorption capacity of the crystalline phase of sPS has been estimated to be about 20 times larger than that of the amorphous phase.[13]

As anticipated above, also the sorption capacity of semicrystalline nanoporous PPO has been reported to be significantly larger than that of totally amorphous PPO:[7] by taking advantage of such feature and by considering the relatively high diffusion coefficients measured, semicrystalline forms of PPO could be considered as suitable for use in membrane-based gas separation processes, where polymers that exhibit large values of permeability are required to guarantee high permeate fluxes. In general, any modification aimed at enhancing gas permeability is accompanied, both in neat polymers and in glassy polymers loaded with inorganic fillers,[21] by a decrease of selectivity. There is, then, a trade off between permeability and selectivity, as indicated by the Robeson upper bound in the selectivity vs permeability plot.[22,23] This issue is specifically addressed in this contribution with reference to the investigated semicrystalline PPOs. In view of its structural peculiarity related to the nanoporous structure of its crystalline domains, semicrystalline nanoporous PPO could be thought of as a special kind of *mixed matrix membrane* (MMM),[24−28] because the presence of crystalline domains acts by improving the gas transport properties, just as in the case of MMMs which are instead obtained by adding inorganic nanoparticles to polymer matrices. This aspect is of practical concern, since adding inorganic particles to polymers to improve the overall transport rate often causes a series of problems, among which the poor adhesion between polymer and filler is of particular relevance, since it leads to the formation of defective interphases. Moreover, in the case of porous fillers, like zeolites, the polymer chains can determine the blockage of pores and channels, reducing the benefits given by the inorganic phase. Conversely, the use of nanoporous semicrystalline polymers could avoid such problems since it would not require to couple the polymer matrix to an inorganic species: simply, by proper choosing the guest solvent and the process conditions for the treatment of amorphous PPO, it would be possible to tailor the fine structure of the nanoporous crystalline domains, limiting at the same time the formation of structural defects.

In the present contribution attention is focused on semicrystalline PPO, which is characterized by even larger gas permeability levels as compared to semicrystalline sPS, supplying a detailed analysis of mass transport properties in amorphous and semicrystalline samples and by highlighting the role played by the solvent used for the crystallization treatment and, in turn, by the associated nanoporous structure of crystalline phase in semicrystalline PPO.

2. THEORETICAL BACKGROUND

2.1. Permeability and Selectivity. The permeability of a polymer film to a gas or vapor penetrant is defined as the ratio between the penetrant flux, J, and the trans-membrane pressure gradient, according to the relationship[29]

$$P = \frac{J}{\Delta p/l} \tag{2}$$

where l is the membrane thickness. Permeability is commonly expressed in Barrers, where 1 barrer $=10^{-10}$ (cm^3(STP)·cm)/(cm^2·cmHg·s). When the solution-diffusion model holds and the sorption kinetics follow the Fick's law, the permeability can be estimated from sorption tests using the following expression:

$$P = S \times \bar{D} \tag{3}$$

Here S is the solubility coefficient and $\bar{D}$ the concentration-averaged penetrant diffusivity.

Besides permeability, another key parameter in membrane separation processes is the ideal selectivity, α_{ij}, defined, when the downstream pressure is much lower than that of the feed, as the ratio between the permeability of pure components i and j, i.e., P_i and P_j:

$$\alpha_{ij} = \frac{P_i}{P_j} = \left(\frac{S_i}{S_j}\right) \times \left(\frac{\bar{D}_i}{\bar{D}_j}\right) \tag{4}$$

It is noticed here that, as reported by several authors, the values of ideal selectivity obtained from pure vapor sorption or permeation data could be different from the real selectivity for gas or vapors mixtures, in the cases in which interactions take place among the penetrants and between the penetrants and the membrane material, and when the transport process is accompanied by significant matrix swelling.[30,31]

On the basis of solution-diffusion model, the ideal selectivity can be factored into two different contributions, namely solubility-selectivity (i.e., S_i/S_j) and diffusivity-selectivity (i.e., $\bar{D}_i/\bar{D}_j$). Usually, the diffusivity selectivity is the dominating term in glassy polymers that exhibit medium-low free volume fractions, while in high free volume glassy polymers the opposite behavior is observed, the overall selectivity being controlled by the solubility contribution. In the first case, one has the well-known size-sieving effect, in view of the fact that the selectivity is favorable to the lower molecular size components, while in the latter case the larger vapors, that are more soluble and condensable, result to be also more permeable.[30−32] In view of the fact that the solubility coefficient increases with the penetrant critical temperature, the solubility selectivity strongly depends on the difference of condensability between the penetrants considered.[33] On the other hand, the

dx.doi.org/10.1021/ma3000626 | Macromolecules 2012, 45, 3604−3615

diffusivity of lighter and less condensable gases is systematically higher than the one of larger size vapors. Then, a trade off exists between solubility selectivity and diffusivity selectivity: it is clear that the knowledge of both such parameters is of crucial importance in designing high performance membrane modules.[34]

2.2. Sorption Thermodynamics. Different models have been proposed to describe the sorption isotherms in amorphous glassy polymers: the dual mode sorption model[35] is certainly one of most widely known and used approaches to correlate both pure and mixed gas solubility in a wide series of glassy matrices.[36,37] Drawbacks of this simple model are, however, that it is not amenable to a predictive use and that the set of parameters determined from sorption data are often unable to describe the corresponding desorption isotherms.[37]

In the last two decades, more advanced models appeared in literature. Among them we consider in detail here the *nonequilibrium lattice fluid* (NELF) model, proposed by Doghieri and Sarti,[38] that, on the roots of rational thermodynamics, extended the Sanchez–Lacombe theory,[39,40] developed for equilibrium rubbery polymers, to the nonequilibrium case of glassy polymers, by choosing a proper order parameter to account for the departure of glassy state from the equilibrium conditions.[38,41,42] In particular, the polymer density, ρ_2, is used as an order parameter, in view of the fact that it gives a direct measurement of the degree of nonequilibrium of the glassy system. Differently from the case of equilibrium rubbery polymers, density of the polymer in the glassy-polymer/low molecular weight penetrant mixture cannot be retrieved from calculations based on equations of state. In fact ρ_2 plays the role of an internal state variable, which evolves at a rate that is dependent on the nonequilibrium values of state variables of the system. To simplify the matter, avoiding involvement of kinetics issues, in the application of NELF theory it is generally assumed that polymer density is frozen-in at the starting value of the unpenetrated glassy polymer, i.e., that its evolution kinetics is much slower than that characteristic of the gas sorption process.

On the basis of this approach, Doghieri and Sarti,[38,41,42] proposed the following expression for the chemical potential of a low molecular weight penetrant absorbed within a glassy polymer:

$$\mu_1^S(T, p, \omega_1, \rho_2) = \left(\frac{\partial G}{\partial n_1}\right)_{T,p,\rho_2,n_2} = RT\ln(\tilde{\rho}\phi_1) - RT\left[r_1^0 + \frac{r_1 - r_1^0}{\tilde{\rho}}\right]\ln(1-\tilde{\rho}) - r_1 + \tilde{\rho}[r_1^0 v^*_1(p^*_1 - p^* - \phi_2^2\Delta p^*)] \quad (5)$$

On this basis, the *pseudo phase equilibrium* between a pure gas penetrant phase and the penetrant absorbed in the glassy polymer phase can be hence obtained by equating the chemical potential of the penetrant in the external gaseous phase to that given by eq 5. The term *pseudoequilibrium* is used here in view of the fact that the phase equilibrium is attained for an apparently constant value of polymer density that is, actually, a nonequilibrium property.

In eq 5, the subscripts 1 and 2 stand for gas and polymer respectively, ω_i and ϕ_1 represent the mass and the volume fraction respectively of the component ith in mixture, r_1^0 and r_1 are the number of lattice sites occupied by a gas molecule in the pure state and in the glassy mixture, and $\tilde{\rho}$ is the mixture reduced density, defined as the ratio

$$\tilde{\rho} = \frac{\rho}{\rho^*} \quad (6)$$

where ρ is the density of polymer phase mixture and ρ^* a characteristic mixture parameter. The value of ρ can be calculated from the value of polymer density, ρ_2, by the following expression:

$$\rho = \frac{\rho_2}{\omega_2} \quad (7)$$

Finally, p^*_i and v^*_i are equation of state parameters for the pure species. The characteristic pressure, p^*, of the glassy polymer mixture can be calculated from the corresponding values for pure components, p^*_1 and p^*_2, through the following mixing rule:

$$p^* = \phi_1 p^*_1 + \phi_2 p^*_2 - \phi_1\phi_2(1 - k_{ij})(\sqrt{p^*_1} - \sqrt{p^*_2})^2 \quad (8)$$

The parameters p^*_1, p^*_2, and p^* are related to the cohesive energy density of species 1 and 2 and of the mixture, respectively; hence, they give an estimate of the extent of self- and mutual mean field interactions. In eq 8, k_{ij} represents an adjustable parameter that can be optimized on the basis of experimental solubility data, when available. Alternatively, it can be, in a first approximation, fixed to be equal to zero.[43] From a physical point of view, k_{ij} measures the deviation from the empirical geometric mean combination rule for p^*. Finally, v^*_i is related to a characteristic temperature of the substance through the relationship:

$$v^*_i = \frac{RT^*_i}{p^*_i} \quad (9)$$

Obviously, use of the NELF model requires the *a priori* knowledge of the characteristic parameters p^*_i, T^*_i, and ρ^*_i for both the penetrant and the polymer species: for the penetrant, they can be obtained by fitting experimental equilibrium liquid–vapor data with the Sanchez–Lacombe equation of state,[39] while for the polymer they can be determined by fitting, to the same equation of state, the experimental *PVT* data in the rubbery region, where equilibrium conditions hold (more on this later).

It is important to note that, in presence of swelling penetrants, one needs also to account for possible 'instantaneous' changes of the nonequilibrium frozen-in polymer density. In fact, in such cases the polymer density experiences a nonnegligible change, as long as the sorption proceeds, to accommodate penetrant molecules: experimental data collected on different systems suggest that the starting value of ρ_2 decreases linearly with the penetrant partial pressure,[44] according to the relationship

$$\rho_2 = \rho_2^0(1 - k_{sw}p) \quad (10)$$

where ρ_2^0 is the density of the pure unpenetrated polymer phase and k_{sw} is a swelling coefficient, that can be obtained directly from dilation experiments[45] or, indirectly, from the analysis of experimental solubility isotherms at relatively high pressures, where the swelling extent is larger, according to the procedure reported by Giacinti et al.[46] Here ρ_2 still represents a kinetically

dx.doi.org/10.1021/ma3000626 | Macromolecules 2012, 45, 3604–3615

frozen value of polymer density, which is different from the starting frozen-in density of pure glassy polymer since room is necessary to accommodate penetrant molecules. Conversely, sorption of nonswelling penetrants does not induce any appreciable variation of the matrix density and the entire sorption isotherm can be correctly predicted by imposing the swelling coefficient equal to zero and using k_{ij} as the only fitting parameter.

3. EXPERIMENTAL SECTION

3.1. Materials. The PPO used in this study was purchased by Sigma-Aldrich and presents weight-averaged and number-averaged molecular masses M_w= 59000 and M_n= 17000, respectively. Solvents used to prepare the semicrystalline samples (i.e., benzene and carbon tetrachloride) were purchased from Aldrich and used without further purification. For gas sorption measurements, high purity gases (>99.6%) supplied by Rivoira (Chivasso, Italy) were used as received.

PPO amorphous (in the following aPPO) films were obtained by compression molding after melting at 290 °C. The crystallization of these amorphous films has been induced by contacting them with vapors of different solvents at room temperature. The solvent was then removed from the crystallized films by treatment with a SFX 200 supercritical carbon dioxide extractor (ISCO Inc.), at 40 °C and 250 bar, with an extraction time of 300 min. Two different types of semicrystalline PPO samples were obtained by using two different solvents: bPPO, obtained by treatment with benzene and cPPO obtained by treatment with carbon tetrachloride.

3.2. X-ray, FTIR, and DSC Characterization. X-ray diffraction patterns were obtained on a Bruker D8 Advance automatic diffractometer operating with a nickel-filtered Cu Kα radiation. The degree of crystallinity of nanoporosous films was obtained from the X-ray diffraction data, by applying the standard procedure of resolving the diffraction pattern into two areas corresponding to the contributions of the crystalline and amorphous fractions.

Fourier transform infrared (FTIR) spectra were obtained at a resolution of 2.0 cm^{-1} with a Tensor 27 Bruker spectrometer equipped with deuterated triglycine sulfate (DTGS) detector and a Ge/KBr beam splitter. The frequency scale was internally calibrated to 0.01 cm^{-1} using a He−Ne laser. A total of 32 scans were signal averaged to reduce the noise.

The infrared based degree of crystallinity, X_C, can be evaluated according to the following relationship:[47,48]

$$K = \frac{l}{l'(1 - X_C)} \tag{11}$$

Here K is the subtraction coefficient used to reduce to baseline the contribution of the amorphous phase, l and l' are the thickness of the sample and of an amorphous PPO reference film. The ratio l/l' was estimated from the absorbance ratio of a conformationally insensitive peak, i.e., at 960 cm^{-1}.

Differential scanning calorimetry (DSC) analysis has been performed on amorphous and semicrystalline samples of PPO to gather information on glass transition and melting temperatures as well as, only for the semicrystalline samples, on enthalpy of melting. Test were performed on samples of around 10 mg sealed in a nonhermetic aluminum pan and under nitrogen atmosphere by using a Q1000 DSC apparatus (by TA Instruments, New Castle, DE) at a temperature scanning rate of 5 °C/min in the temperature range from 25 to 400 °C.

3.3. Sorption Measurements. Subatmospheric sorption experiments were carried out using a CAHN D200 electronic microbalance (CAHN Instruments, Madison, WI), with a sensitivity of 0.1 μg. The weighing unit element is put at the top of a close water-jacketed glass chamber containing the polymer sample hanged at the left arm of the balance, while an inert tare is suspended on the opposite arm, enclosed in a stainless steel case. All the system is vacuum tight, connected with service lines to the gas feeding system, to the vacuum pump and to the exhaust. The sampling chamber is thermostated with a water jacket equipped with a recirculation pump, to keep the temperature constant to within ±0.1 °C, while the pressure is monitored by a Baratron 121A (MKS Instruments, Andover, MA) manometer with a full scale of 1000 Torr, a resolution of 0.01% of the full scale range and an accuracy of 0.5% of the reading.

The experiments were performed by step increasing the penetrant partial pressure, after equilibrium conditions was reached at the previous sorption step: by following this procedure, the solubility and diffusivity values were determined in a stepwise manner, as a function of penetrant partial pressure. In particular, the gas solubility, expressed as grams of sorbed gas per gram of polymer, was estimated from the analysis of equilibrium sorption stage, while the diffusivity was retrieved from the analysis of the transient sorption stage, by assuming a Fickian behavior: this hypothesis was verified by fitting the experimental transient sorption data with the rigorous solution of the penetrant mass balance equation, for one-dimensional geometry. The evaluation of diffusion coefficients has been performed on the basis of the simplified linear correlation holding, for systems following Fick's law, between the mass absorbed and the square root of time, which is quite accurate up to sorption times for which the mass absorbed does not exceed the 60% of the total value[49] (i.e., $M_t/M_\infty < 0.6$), i.e.:

$$\frac{d(M_t/M_\infty)}{dt^{1/2}} = \left(\frac{16D}{l^2\pi}\right)^{1/2} \tag{12}$$

where D is the gas-polymer mutual diffusivity, M_t and M_∞ are the mass of penetrant absorbed at the time t and at equilibrium conditions, respectively, and l is the film thickness, that was estimated with a digital micrometer with an accuracy of ±1 μm. In applying eq 12 it has been assumed that diffusivity, during each sorption step, is rather constant in view of the limited associated step increase in pressure and, in turn, of the limited penetrant concentration change within the polymer.

It has to be noted here that, in view of the heterogeneous nature of the semicrystalline PPOs, the values of diffusivity determined for these samples are to be considered as spatial averages over the volume of the sample which reflects both the mass transport properties of the amorphous and of the crystalline domains, in a fashion which depends on the detailed morphological structure of the polymer. As a consequence, the reported values have to be considered only for qualitative comparison between amorphous and semicrystalline PPOs. Scaling of these values to PPO samples characterized by a different level of crystallinity and different orientation of crystals could be performed only once detailed information on the crystalline structure will be available.

3.4. PVT Experiments and Density Measurements. The pressure−volume−temperature properties for amorphous PPO were measured using a high pressure dilatometer provided by Gnomix (Boulder, CO).[30] In this apparatus, the polymer sample is kept under hydrostatic pressure using mercury as confining fluid: subsequent compression runs were performed at constant temperature by increasing the pressure in a stepwise manner and recording the corresponding change of polymer volume. When an isothermal compression was completed, the system temperature was increased and a new isothermal run was repeated. In the case at hand, the experiments were performed from 25 °C up to 320 °C, in a pressure range spanning from 0.1 to 100 MPa.

The volumetric data collected for amorphous PPO are reported in Figure 2a, in both rubbery and glassy states. The lattice fluid characteristic parameters were then estimated by fitting the experimental *PVT* data above the glass transition temperature with Sanchez−Lacombe equation of state[39] for pure fluids, i.e.

$$\tilde{\rho} = 1 - \exp\left[-\frac{\tilde{\rho}^2}{\tilde{T}} - \frac{\tilde{p}}{\tilde{T}} - \left(1 - \frac{1}{r}\right)\tilde{\rho}\right] \tag{13}$$

where $\tilde{\rho} = \rho/\rho^*$, $\tilde{T} = T/T^*$, and $\tilde{p} = p/p^*$. The values determined by a best fitting procedure for p^*, T^*, and ρ^* for amorphous PPO are reported in Table 1.

dx.doi.org/10.1021/ma3000626 | Macromolecules 2012, 45, 3604−3615

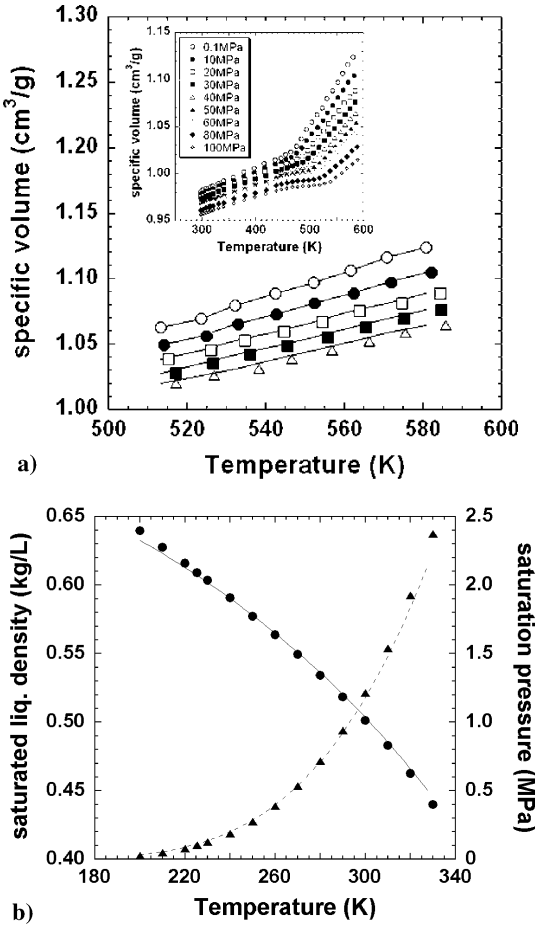

Figure 2. (a) Fitting of experimental PVT data to Sanchez–Lacombe equation of state for aPPO; (b) fitting of equilibrium data for propylene (●, saturated liquid density; ▲, vapor pressure) to Sanchez–Lacombe equation of state.

As observed by several authors,[51,52] the Sanchez–Lacombe equation of state is often unable to describe using a single set of parameters the volumetric properties of polymers with adequate reliability over very wide ranges of temperature and pressure. Hence, to improve the accuracy of the model in representing volumetric properties, data fitting with the Sanchez–Lacombe equation of state was performed in a range of experimental data close to the temperatures and pressures of interest: in fact, in this investigation, just the *PVT* data ranging from 0.1 to 40 MPa were used to retrieve the Sanchez–Lacombe parameters of amorphous PPO.

The lattice-fluid parameters of methane, carbon dioxide, and propane were taken from literature sources,[38,41−43] while, in the case of propylene, they were estimated by fitting simultaneously the vapor pressure and the saturated liquid density as a function of temperature to the Sanchez–Lacombe equation of state; to this aim, the experimental data for propylene were taken from technical literature.[53] The results of fitting for propylene are reported in Figure 2b, while in Table 1 are reported the calculated values for lattice-fluid parameters. As expected, the lattice-fluid scaling parameters for propylene do not depart very much from those of propane.

The density of amorphous and semicrystalline PPO was accurately measured by flotation at environment temperature and pressure. These values have been used: (a) to obtain absolute values of polymer density needed to compute the absolute PVT behavior of PPO, in view of the fact that Gnomix apparatus only supplies volume changes; (b) as the value of ρ_2 to be used in applying NELF model to aPPO; and (c) to convert the mass fraction of gas in volume fractions.

Parallel flotation experiments have showed that the density of totally amorphous PPO (1.016 ± 0.004 g/cm^3) is slightly higher than the one of the semicrystalline sample obtained after treatment with benzene (1.009 ± 0.002 g/cm^3): such result appears rather unusual and, as we will see later, it is consistent with the results of sorption experiments. A similar behavior has been previously observed in the case of semicrystalline syndiotactic polystyrene.[13] Unfortunately, it was not possible to estimate the density of cPPO due to the morphology of samples, which did not allow a reliable use of the flotation procedure. In fact, the samples crystallized with CCl_4 displayed a quite irregular shape which determined trapping of bubbles in the suspending solution around the sample. Since the value of density is needed to calculate *S* (appearing in eq 3) starting from the experimental values of solubility as a function of pressure, no estimate of permeability from eq 3 has been possible for cPPO. For this reason, in the following, the comparison of cPPO with bPPO will only be performed with reference to sorption behavior.

4. RESULTS AND DISCUSSION

4.1. X-ray, IR, and DSC Characterization. The X-ray diffraction patterns of aPPO, bPPO and cPPO film samples are shown in Figure 3. As already reported in a previous work,[7] the

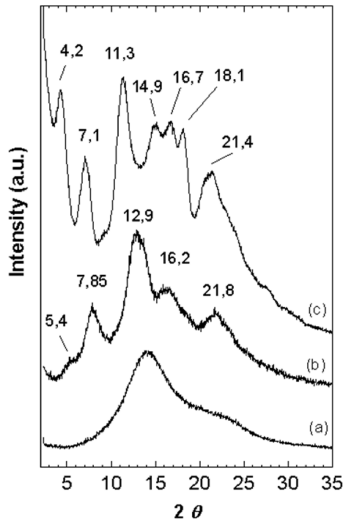

Figure 3. X-ray diffraction patterns of aPPO (curve a) and semicrystalline bPPO (curve b) and cPPO (curve c) film samples.

X-ray diffraction patterns of bPPO and cPPO films present peaks being located at definitely different diffraction angles

Table 1. NELF Model Parameters for aPPO, Penetrants, and Their Mixtures

	T^* (K)	p^* (MPa)	ρ^* (kg/L)	source	T_C (K)	V_C (cm^3/mol)	k_{sw} (MPa^{-1})	k_{ij}
aPPO	703	510	1.135	this work	–	–	–	–
C_3H_8	375	320	0.690	ref 43	369.8	203	0.044	0.035
C_3H_6	392	300	0.700	this work	364.9	181	0.042	0.007
CH_4	215	250	0.500	ref 41	190.4	99.2	≈0	−0.018
CO_2	300	630	1.515	ref 38	304.1	94	0.015	0.030

dx.doi.org/10.1021/ma3000626 | *Macromolecules* 2012, 45, 3604−3615

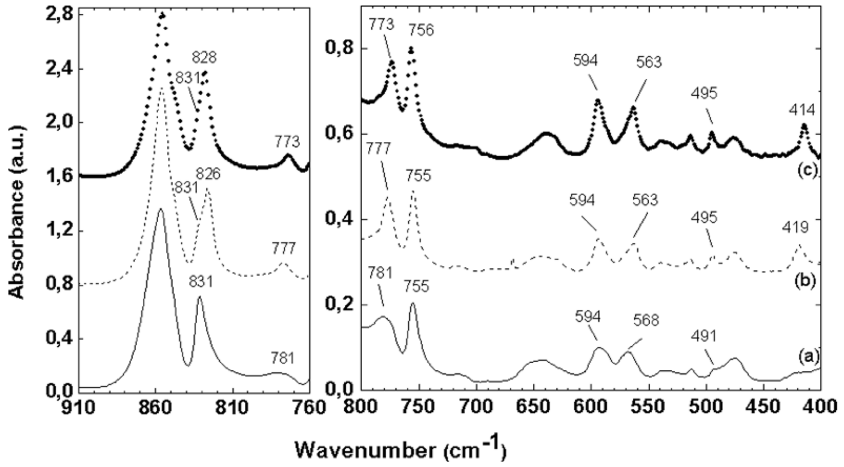

Figure 4. IR spectra of a aPPO film sample (curve a) and bPPO (curve b) and cPPO (curve c) film samples. The 910−400 cm^{-1} wavenumber region has been split in two graphs for the sake of clarity.

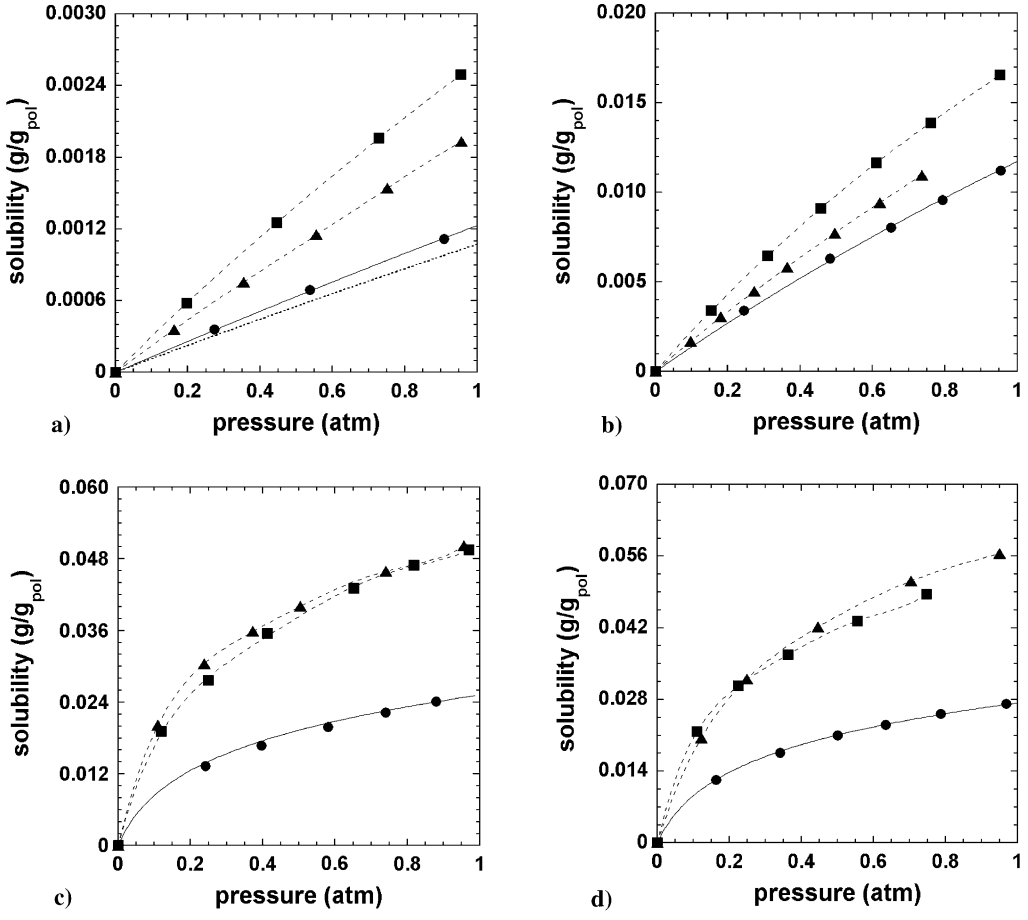

Figure 5. Sorption isotherms at 30 °C for (a) CH_4, (b) CO_2, (c) C_3H_8, and (d) C_3H_6 in aPPO (●), bPPO (■), and cPPO (▲). Continuous lines (−) represent two-parameters NELF model fitting. Dotted line (···), only in the case of methane, represents NELF model prediction with no fitting parameters. Dashed lines (---) are only guides for the eye.

which indicate the formation of different crystalline modifications. Both modifications, according to molecular sorption and surface area measurements, are nanoporous.

In Figure 4 are reported the IR spectra in the 910−400 cm^{-1} wavenumber range of amorphous and semicrystalline PPO films, whose X-ray diffraction patterns have been reported in Figure 3. As can be observed, the IR spectrum of fully amorphous PPO sample (curve a) in the 910−400 cm^{-1} region is markedly different from those of both semicrystalline PPO samples. In particular: (i) the broad bands of aPPO located at 781, 594, 563, and 491 cm^{-1} become sharper in semicrystalline samples; (ii) in the 410−420 cm^{-1} region, the semicrystalline samples display a sharp IR band which is negligible in the aPPO; (iii) the IR spectrum of aPPO presents a sharp band at 831 cm^{-1} which becomes, in semicrystalline PPO samples, the shoulder of a new band located at a lower wavenumber.

dx.doi.org/10.1021/ma3000626 | *Macromolecules* 2012, 45, 3604−3615

Following an approach developed for syndiotactic polystyrene, the degree of crystallinity of semicrystalline PPO samples has been determined by subtracting the contribution of the amorphous phase. The spectral subtraction was accomplished by choosing the K parameter (see Experimental Section) so as to reduce the typical aPPO band at 831 cm^{-1} to the baseline. The degree of crystallinity, was found to be 32% for both the samples crystallized with benzene and carbon tetrachloride. This indicates that the amount of polymer chains in ordered conformation is similar for the two nanoporous-crystalline samples.

It is worth adding that for the crystalline sample obtained by treating aPPO with benzene the degree of crystallinity determined from the X-ray diffraction pattern (curve b of Figure 3) by applying the standard procedure of resolving the diffraction pattern into two areas corresponding to the contribution of the crystalline and amorphous fractions was found to be 32% which is similar to the value obtained from the IR spectrum.

Finally, we note that the IR spectra of the two semicrystalline PPO films, although very similar, exhibit significant variations, due to different chain conformation or packing in the nanoporous crystalline phase. In particular, bPPO (curve b) presents peaks located at 826, 777, and 419 cm^{-1} while cPPO (curve c) presents peaks located at 828, 773, and 414 cm^{-1}.

Differential scanning calorimetry has been performed on aPPO, bPPO, and cPPO determining glass transition temperature, T_g, and, for semicrystalline samples, melting temperature, T_m, and melting enthalpy of the crystalline phase, ΔH_m. Values of T_g resulted, for all the samples, around 211 °C, thus suggesting that the presence of crystals does not alter significantly the mobility of the amorphous phase. Melting temperatures were also very close for the two semicrystalline samples. In particular, for the case of bPPO it was determined T_m = 239.6 °C and a melting enthalpy equal to 12.8 J/g, that corresponds to a ΔH_m for the crystal equal to 1.16 kcal/mol. On the basis of this information, the entropy of melting of the crystal, ΔS_m, was estimated to be 2.27 cal/(mol K), from the relationship $\Delta S_m = \Delta H_m/T_m$. Both the value of ΔH_m and of ΔS_m are lower than those generally found in semicrystalline polymers.[15] This result points to weak interchain interactions, consistently with the hypothesis of a nanoporous crystalline phase, aspect that has already been evidenced by Alentiev et al.[15] in their investigation on semicrystalline PPO.

4.2. Solubility. Sorption experiments of methane, carbon dioxide, propane, and propylene were performed at 30 °C on both aPPO and semicrystalline bPPO and cPPO samples. For all the penetrants investigated, the solubility was determined to be lower for aPPO as compared with semicrystalline PPOs, indicating that the sorption capacity of the whole sample increases after crystallization with solvents: such a behavior is consistent with the lower density showed by the semicrystalline bPPO with respect to the amorphous sample, which points, in turn, to a lower density and higher associated sorption capacity of the crystalline phase. This trend is clearly opposite to the one commonly observed in semicrystalline polymers, where the gas solubility results to be proportional to the volume fraction of the amorphous phase, according to the linear model proposed by Michaels et al.[16−18] In parts a−d of Figures 5 are reported the sorption isotherms for all the penetrants tested in amorphous and semicrystalline PPOs as a function of the penetrant partial pressure: they are concave to the pressure axis for carbon dioxide, propane and propylene, as expected on the basis of the typical behavior of glassy amorphous polymers and of the Langmuir-type adsorption in well-defined nanocavities of crystalline nanoporous structures, while a quite linear trend is observed in the case of methane, likely due to the fact that in this case the absorbed amount at equilibrium is far enough from saturation value. Moreover, the solubility increases systematically with the penetrant critical temperature, following the order $CH_4 < CO_2 < C_3H_6 \approx C_3H_8$.

In particular, by reporting for each penetrant the logarithm of experimental solubility coefficient at infinite dilution in amorphous PPO as a function of the penetrant critical temperature, a good linear trend is observed, that can be rigorously justified from the theoretical point of view on the basis the NELF model.[33] In Figure 6 is reported a comparison

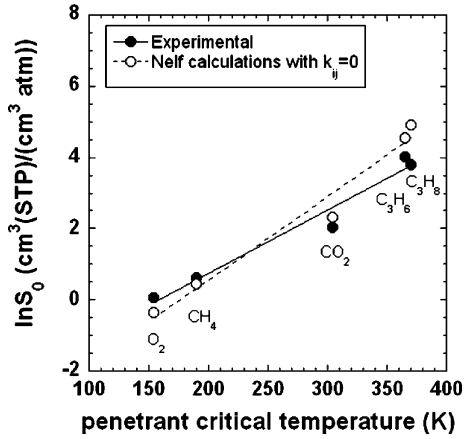

Figure 6. Experimental and calculated solubility coefficients at infinite dilution in aPPO as a function of penetrant critical temperature.

between experimental and theoretical solubility coefficients at infinite dilution (as predicted by using NELF model with k_{ij} = 0) as a function of the penetrant critical temperature which shows that the NELF model is able to give a reasonable representation of the linear trend displayed by experimental data: the greater departure showed by the theoretical values with respect to the experimental data in the case of larger hydrocarbons can be justified by considering that, to use NELF model in a predictive fashion, the binary interaction parameter has been set equal to zero. The experimental infinite dilution solubility S_0 was calculated for each penetrant by extrapolating at vanishing pressure the experimental solubility coefficient, i.e.

$$S_0 = \lim_{p \to 0}\left(\frac{C}{p}\right) \tag{14}$$

where C is the gas concentration expressed in $cm^3(STP)/cm^3$ and p the respective equilibrium pressure. In Figure 6 the value of S_0 at 30 °C for oxygen (T_C =154.6 K), taken from literature sources,[33] was also represented for comparison purposes.

The entire experimental sorption isotherms in aPPO were also compared with the theoretical predictions of NELF model, whose scaling parameters for the polymer species were estimated by fitting the experimental PVT data to the Sanchez−Lacombe equation of state, according to the procedure described above. As is shown in Figures 5a-d, the model provides a very good fitting of experimental data in the whole pressure range inspected and for all the penetrants. For nonswelling penetrants, methane in our case, only k_{ij} was used as fitting parameter, assuming k_{sw} = 0.

dx.doi.org/10.1021/ma3000626 | Macromolecules 2012, 45, 3604−3615

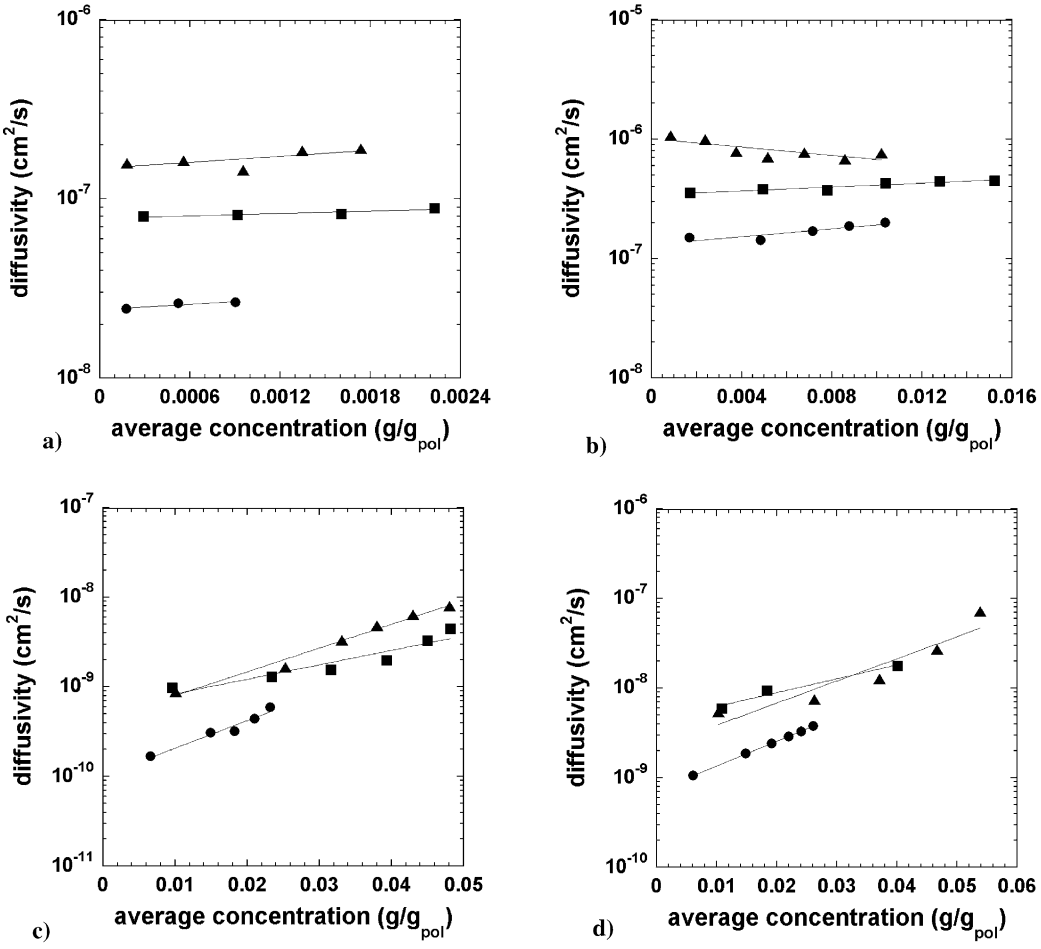

Figure 7. Diffusivity isotherms at 30 °C for (a) CH_4, (b) CO_2, (c) C_3H_8, and (d) C_3H_6 in aPPO (●), bPPO (■), and cPPO (▲). Continuous lines represent an exponential interpolation.

Conversely, for swelling penetrants, i.e. carbon dioxide, propane and propylene, both k_{ij} and k_{sw} were used as fitting parameters: in particular, the latter was determined following the procedure proposed by Giacinti et al.[45] In other words, by taking advantage of the linear relationship holding for the polymer density as a function of the penetrant partial pressure, the swelling coefficient can be retrieved by applying eq 10, i.e.:

$$k_{sw} = \left[\frac{\rho_2^0 - \rho_2(p)}{\rho_2^0}\right]\frac{1}{p} \tag{15}$$

where ρ_2^0 is the pure polymer density before sorption experiments, that is known from density measurements, and ρ_2 the density at pressure p, as retrieved by fitting the corresponding solubility datum with the NELF model. For all the swelling penetrants tested, the corresponding value of k_{sw} was optimized using the solubility datum available at the highest pressure. The binary interaction parameter as well the swelling coefficient determined by the fitting procedure for each polymer/penetrant couple are reported in Table 1. As a matter of fact, the values of k_{ij} do not depart very much from zero for all the polymer/penetrant pairs. Moreover, the experimental solubility data for methane are reasonably represented by the NELF model also when it is used in a completely predictive way, i.e., by setting the binary parameter identically equal to zero: a comparison between the two different modeling approaches ($k_{ij} = 0$ and $k_{ij} \neq 0$) for nonswelling penetrant (CH_4) is reported in Figure 5a.

The extent of swelling, as calculated through the NELF model, follows the order $CO_2 < C_3H_6 \approx C_3H_8$, consistently with the lower molecular size of carbon dioxide with respect to the hydrocarbon vapors. In all the cases, however, the amorphous sample shows a very good dimensional stability, in view of the fact that the percentage volume dilation induced by sorption of propane does not exceed the 0.45% at atmospheric pressure, as it is possible to estimate from the respective values of k_{sw}: such aspect is of crucial importance in separation processes, where materials endowed with adequate dimensional stability are required.

As anticipated above, semicrystalline PPOs display a higher sorption capacity than aPPO, due to their ability to host gas molecules in their crystalline nanocavities, according to a Langmuir-type adsorption mechanism. We did not attempt to retrieve quantitative information on gas solubility in the pure crystalline phase from sorption isotherms for semicrystalline PPOs and aPPO. In fact, for the amorphous phase of semicrystalline PPOs, the assumption of the same solubility of aPPO, which is needed to perform this calculation, is not necessarily fair.

It is noticed that, by comparing the mass transport properties of bPPO and cPPO, no appreciable differences were found in the case of propane and propylene: in these cases, the same solubility was measured in the two semicrystalline matrices,

dx.doi.org/10.1021/ma3000626 | Macromolecules 2012, 45, 3604−3615

that, in turn, results roughly doubled with respect to the one measured in the aPPO. Conversely, by considering carbon dioxide and methane, nonnegligible differences emerged between the solubilities in bPPO and cPPO: for instance, in the case of methane the solubility in bPPO results about double than in aPPO, while the solubility in cPPO is roughly 1.5 times larger than the one measured in the amorphous sample. Analogously, in the case of carbon dioxide the sorption capacity of bPPO is about 1.5 times larger than that of aPPO, while for cPPO this ratio reduces to 1.2. In summary, for the more condensable hydrocarbons both the semicrystalline matrices show the same sorption capacity, while for the less condensable gases a rather different solubility was measured in bPPO and cPPO.

4.3. Diffusivity. For all the penetrants tested, a Fickian behavior was observed during the transient sorption stage and, on the basis of eq 12, the average diffusivity was estimated as a function of penetrant average concentration: the results are reported in Figure 7a–d for amorphous and semicrystalline PPOs. We remark here that, as already pointed out in the Experimental Section, the calculated values of diffusivity for semicrystalline PPOs have to be considered as a spatially averaged property, in view of the heterogeneous nature of the sample. No attempt was made to calculate values of diffusivity for the pure crystalline phase since details on the structure and orientation of the crystalline domains have not been yet fully clarified.

Very interestingly, a significant increase of the diffusivity was observed for all penetrants by moving from amorphous to semicrystalline PPO: this behavior is consistent with the experimental density data of polymer samples and can be attributed to the nanoporous nature of crystalline domains. The values of diffusivities suggest that, in mass transport processes, the semicrystalline phases of PPO keep the size sieving effect proper of amorphous PPO, by promoting a more rapid diffusion for lighter gases. The relevant result of larger diffusivities for semicrystalline PPOs as compared to aPPO appears quite unexpected in view of the fact that usually the presence of semicrystalline regions act by increasing the tortuosity of the penetrant molecular path thus reducing the diffusivity. In fact, generally, crystallites do not contribute to the sorption and diffusion processes, acting like a constraint for the amorphous phase and as a geometrical obstacle to diffusion. In the present case the picture is rather different, because the crystalline phase evidently takes part to the sorption and transport processes, as a consequence of its nanoporous structure, with mass transport rates even higher than those proper of the amorphous domains.

It is explicitly noticed here that, although also for semicrystalline sPS with nanoporous crystalline phases the solubility of low molecular weight compounds has been reported to be significantly higher than in the amorphous sPS,[8,11−14] the distinguishable feature of a higher diffusivity for low molecular weight compounds in the semicrystalline samples is present only in the case of PPO.

As expected, in both amorphous and semicrystalline PPO the diffusion coefficient results to be strongly dependent on the penetrant size: the lowest values for diffusivity were measured in the case of propane, that is the larger sized penetrant inspected, while the highest diffusivities were obtained in the case of carbon dioxide. As it is well-known, the penetrant critical volume is a good scaling parameter to compare the diffusivities of different gases in polymer matrices: indeed by reporting the infinite dilution diffusivity at 30 °C in aPPO, extrapolated from the experimental diffusivity isotherms, as a function of critical volume for all the gas and vapors tested, a monotonous decreasing trend was found, as shown in Figure 8.

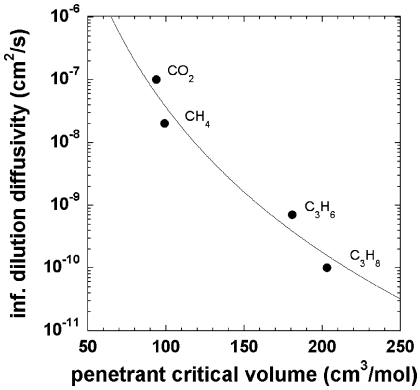

Figure 8. Infinite dilution diffusivity in aPPO as a function of penetrant critical volume.

Finally, it is observed that the diffusivity in all samples increases exponentially with the concentration, specially for propane and propylene. This effect is likely related to the behavior of amorphous domains as a consequence of the matrix dilation: such behavior is consistent with the NELF calculations, which indicates that hydrocarbon vapors induce the higher matrix swelling. A completely different behavior is showed by methane, due to its poor ability to swell the polymer matrix: in this case the diffusivity does not change very much with the penetrant concentration.

4.4. Permeability and Ideal Selectivity. The gas permeabilities of aPPO and bPPO were estimated as the product $\bar{D} \times S$, according to eq 3: as expected on the basis of sorption data discussed above, for each penetrant the permeability increases moving from amorphous to semicrystalline sample. A comparison among the different penetrants tested shows that the permeability is a decreasing function of the penetrant critical volume, just like the diffusivity, and indeed it follows the order $C_3H_8 < C_3H_6 < CH_4 < CO_2$.

Moreover, the analysis of ideal selectivities clearly reveals for aPPO and bPPO a diffusivity-controlled permeability: for example, at 0.24 atm the ideal selectivity CO_2/C_3H_8 is 225, corresponding to a diffusivity selectivity of 970 and a solubility-selectivity of 0.23. This result clearly indicates that, though the solubility selectivity is favorable to the more condensable penetrant, i.e., C_3H_8, the selectivity is globally favorable to CO_2, as a consequence of the diffusivity contribution.

Also for the couple CO_2/CH_4 a size sieving effect was observed: in particular, the total ideal selectivity for carbon dioxide was calculated to be about 20 in aPPO, in good agreement with previous results reported in literature.[1] In Figure 9 the ideal selectivity CO_2/CH_4 calculated for both aPPO and bPPO is represented as a function of CO_2 permeability and compared with the values reported in literature for PTMSP,[54] 6FDA-based polyimides[55] and TR (thermally rearranged) polymers:[56] the latter matrices, containing benzoxazole-phenylene or benzothiazole-phenylene structures, exhibit an exceptionally high separation ability for the pair CO_2/CH_4 in view of the fact that their performances can reach and overcome the upper bound calculated by Robeson[28] in 2008. Such comparative analysis suggests that the

dx.doi.org/10.1021/ma3000626 | Macromolecules 2012, 45, 3604−3615

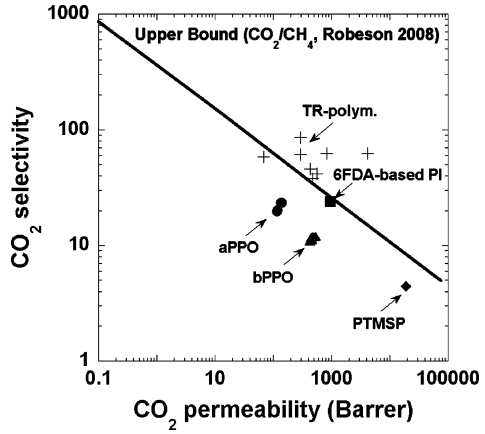

Figure 9. Selectivity–permeability diagram for the mixture carbon dioxide-methane in aPPO, bPPO, and other polymers.

separation capability of both aPPO and bPPO, although lower than those offered by TR polymers or 6FDA-based polyimides, are still better than those showed by PTMSP in term of selectivity. Moreover, because of the low pressure reached in the sorption experiments (<1 atm), it is reasonable to assume that the ideal selectivities estimated from pure gas sorption data do not differ very much from the actual values in mixed gas conditions, as also suggested by Robeson.[28]

A comparison among the permeation properties of aPPO and bPPO for the CO_2/CH_4 mixture reveals that the ideal selectivity decreases moving from amorphous to semicrystalline sample, as shown in the same Figure 9: such loss of selectivity is reasonably related to the porosity shown by the crystalline phases of PPO.

An estimation of ideal selectivity was made also for the couple propane–propylene, that is of relevant concern in petrochemical industry: in agreement with previous results reported in literature,[57,58] an ideal selectivity of about 10 for propylene was found for both aPPO and bPPO. Also in this case the selectivity is globally controlled by the diffusivity, which is largely favorable for propylene, in view of the fact that the two vapors show practically the same solubility.

5. EFFECTS OF THERMAL ANNEALING ON GAS TRANSPORT PARAMETERS

Many studies are reported in the literature showing that the mass transport properties of glassy polymers are strongly dependent on their thermal and mechanical history, as well on the film production procedure. For instance, a thermal treatment generally promote the densification of polymer matrix, with a consequent reduction of its sorption capacity and gas permeation rate: this behavior can be attributed to the nonequilibrium state that a polymer experiences below its glass transition temperature.

In this work, samples of aPPO and bPPO were annealed at 65 °C under vacuum for 3 months: after treatment, a sorption run of carbon dioxide and methane was performed on both the samples and the results were compared with those of untreated aPPO and bPPO. Very interestingly, as shown in parts a and b of Figure 10, both solubility and diffusivity resulted unaffected by thermal annealing, indicating a good thermal stability of both amorphous and semicrystalline matrices. Such aspect is of crucial importance, in view of the fact that often a long exposure to medium-high temperatures determines a sensitive

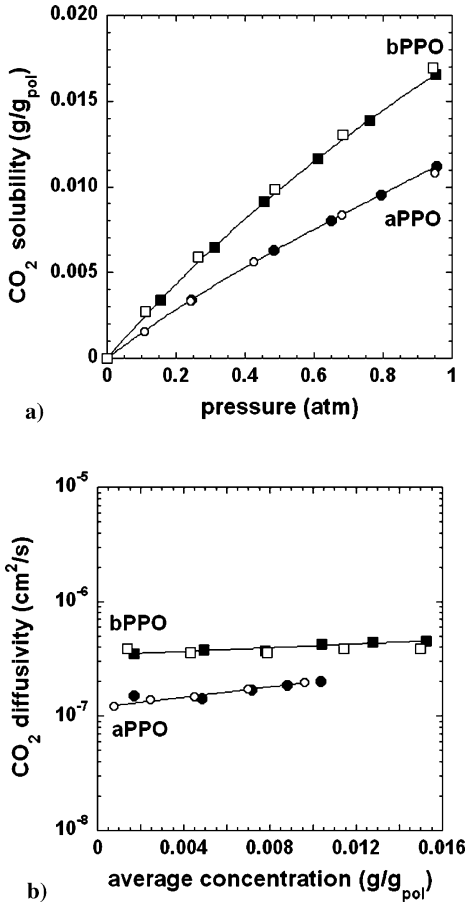

Figure 10. Carbon dioxide solubility (a) and diffusivity (b) isotherms at 30 °C in fresh (filled symbols) and annealed (open symbols) aPPO and bPPO.

reduction of gas transport parameters, like in the case of glassy PTMSP, the most permeable polymer known so far: as observed by Giacinti et al.,[59] indeed, a treatment at 45 °C for 6 month suppresses the solubility of *n*-pentane in PTMSP of about 25%, while a less marked decrease of diffusivity was observed. It is worth noticing that, though both PPO and PTMSP are characterized by high values of the glass transition temperature, the strong instability showed by the latter can be ascribed to its higher degree of free volume, which ranges from 28 to 30%. In parts a and b of Figure 10, the carbon dioxide sorption and diffusion isotherms in fresh and annealed aPPO and bPPO are reported as a function of penetrant partial pressure and penetrant average concentration, respectively: similar results, not reported here for the sake of brevity, were obtained from methane sorption experiments. This behavior is consistent with that reported in literature by Daniel et al.,[7] which observed, at least in the case of large size solvents (C_6H_6, CCl_4), an essentially unaltered uptake after several hours of thermal treatment in air, up to 100 °C.

The good stability showed by PPO can be explained in view of the rigidity of its backbone, related to the presence of the aromatic rings, as well as of its high glass transition temperature, that exceeds that of most of the other glassy polymers, like polystyrene, polycarbonate or polysulphone, coupled with a lower free volume.

dx.doi.org/10.1021/ma3000626 | Macromolecules 2012, 45, 3604–3615

6. DISCUSSION

The unusual behavior of semicrystalline PPO, which displays gas solubility and diffusivity significantly higher than its totally amorphous counterpart, has been rationalized by invoking an involvement of the nanoporous crystalline phase in mass transport. As a matter of fact, there is the possibility that such a behavior could be also ascribed, at least in part, to the existence of a third, amorphous, phase in the semicrystalline samples, beside the bulk amorphous phase and the crystalline phase. This peculiar amorphous domain, originated by the constraint imposed by the crystals on some amorphous regions, has been reported as the "rigid amorphous phase",[60,61] constituted by amorphous backbones with a mobility hindered by the presence of the crystalline phase. An example is the case of the O_2/PET[61] system, for which results of permeation measurements have been rationalized by arguing that the rigid amorphous phase develops an extra excess-hole free volume upon cooling thus promoting a larger oxygen solubility of this amorphous fraction.

In principle, the presence of a rigid amorphous phase could also contribute to the behavior observed for semicrystalline PPO. However, it is to be noted that, at best of our knowledge, there is no case in which a semicrystalline polymer displays higher solubility and diffusivity of low molecular weight compounds as compared to its totally amorphous counterparts. The only relevant exception is the case of semicrystalline sPS samples, exhibiting, in fact, the nanoporous-crystalline δ and ε phases, which present a solubility of suitable guest molecules higher than that of amorphous PS samples, although diffusivities are still lower. In the case of sPS, it has been undoubtedly demonstrated that solubility occurs within the crystalline domains. The presently reported data for PPO actually represent the first case in which both solubility and diffusivity for semicrystalline samples are higher than for the corresponding fully amorphous samples and this finding does speak in favor of a determinant role played by the crystalline regions. Since the structure of the material is, at this stage, not yet resolved, any quantitative prediction of mass transport properties of semicrystalline PPO is not yet possible. Information on the properties of the phases involved as well as on the arrangements of these phases within the sample is needed to obtain macroscopic transport properties by volume averaging. Moreover, preliminary results indicate a large increase of sorption capacity of guest molecules in semicrystalline PPO as a function of grade of crystallinity: this finding, taken together with the results of a detailed structural characterization reported by Daniel et al.[7] in a previous work and of DSC analysis, further supports the fact that the unusual behavior showed by semicrystalline PPO can be mostly attributed to the nanoporous nature of its crystalline phase.

7. CONCLUSIONS

The mass transport properties of amorphous PPO and of semicrystalline nanoporous PPO obtained after treatment with benzene and carbon tetrachloride of aPPO were determined and analyzed for gases and hydrocarbon vapors: the investigated semicrystalline samples are characterized by a gas solubility and diffusivity which are much larger than in the case of totally amorphous PPO. This unexpected behavior can be justified by considering the nonnegligible sorption capacity of the crystalline domains, against what is commonly observed in semicrystalline polymers: such results are further supported by the fact that the density of amorphous PPO is slightly higher than that of semicrystalline samples.

Because of its peculiar mass transport properties, semicrystalline PPO could be a potential candidate for membrane-based gas separation processes: in this respect, interesting values of ideal selectivity were obtained for the pairs CO_2/CH_4 and propylene/propane, which are of strong practical concern in petrochemical industry.

In the case of amorphous PPO, the experimental solubility isotherms compared well with the NELF model calculations, after determination of polymer characteristic parameters: interestingly, the swelling coefficient estimated at atmospheric pressure for more bulky penetrants, namely carbon dioxide, propane, and propylene appear relatively low, indicating a reduced tendency of aPPO to swell in presence of high soluble vapors.

Finally, the mass transport parameters of both amorphous and semicrystalline samples resulted rather insensitive to thermal aging. In fact, a thermal treatment of three months at 65 °C, did not induce any significant change in solubility and diffusivity of carbon dioxide and methane, against what it is commonly observed in other glassy matrices.

AUTHOR INFORMATION

Corresponding Author

*E-mail: michele.galizia@unina.it. Telephone: (+39)-081-7682512. Fax: (+39)-081-7682404.

Notes

The authors declare no competing financial interest.

REFERENCES

(1) Story, B. J.; Koros, W. J. *J. Membr. Sci.* **1992**, *67*, 191.
(2) Ilinitch, O. M.; Semin, G. L.; Chertova, M. V.; Zamaraev, K. I. *J. Membr. Sci.* **1992**, *66*, 1.
(3) Toi, K.; Morel, G.; Paul, D. R. *J. Appl. Polym. Sci.* **1982**, *27*, 2997.
(4) Huang, Y.; Paul, D. R. *J. Polym. Sci. B: Polym. Phys.* **2007**, *45*, 1390.
(5) Wenig, W.; Hammel, R.; MacKnight, W. J.; Karasz, F. E. *Macromolecules* **1976**, *9*, 253.
(6) Barrales-Rienda, J. M.; Fatou, J. M. G. *Kolloid-Z. Z. Polym.* **1971**, *244*, 317.
(7) Daniel, C.; Longo, S.; Fasano, G.; Vitillo, J.; Guerra, G. *Chem. Mater.* **2011**, *23*, 3195.
(8) Manfredi, C.; Del Nobile, M. A.; Mensitieri, G.; Guerra, G.; Rapacciuolo, M. *J. Polym. Sci. B: Polym. Phys.* **1997**, *35*, 133.
(9) De Rosa, C.; Guerra, G.; Petraccone, V.; Pirozzi, B. *Macromolecules* **1997**, *30*, 4147.
(10) Petraccone, V.; Ruiz de Ballesteros, O.; Tarallo, O.; Rizzo, P.; Guerra, G. *Chem. Mater.* **2008**, *20*, 3663.
(11) Rapacciuolo, M.; De Rosa, C.; Guerra, G.; Mensitieri, G.; Apicella, A.; Del Nobile, M. A. *J. Mater. Sci. Lett.* **1991**, *10*, 1084.
(12) Cotugno, S.; Guerra, G.; Mensitieri, G.; Musto, P.; Venditto, V. *Macromolecules* **2002**, *35*, 2296.
(13) Larobina, D.; Sanguigno, L.; Venditto, V.; Guerra, G.; Mensitieri, G. *Polymer* **2004**, *45*, 429.
(14) Mensitieri, G.; Larobina, D.; Guerra, G.; Venditto, V.; Fermeglia, M.; Pricl, S. *J. Polym. Sci. B: Polym. Phys.* **2008**, *46*, 8.
(15) Alentiev, A.; Drioli, E.; Gokzhaev, M.; Golemme, G.; Ilinich, O.; Lapin, A.; Volkov, V.; Yampolskii, Yu. *J. Membr. Sci.* **1998**, *138*, 99.
(16) Michaels, A. S.; Bixler, H. J.; Fein, H. L. *J. Appl. Phys.* **1964**, *35*, 3165.
(17) Michaels, A. S.; Bixler, H. J. *J. Polym. Sci.* **1961**, *50*, 393.
(18) Michaels, A. S.; Bixler, H. J. *J. Polym. Sci.* **1961**, *50*, 413.
(19) Puleo, A. C.; Paul, D. R.; Wong, P. K. *Polymer* **1989**, *30*, 1357.

(20) Pope, D. S.; Koros, W. J. *J. Polym. Sci. B: Polym. Phys.* **1996**, *34*, 1861.
(21) Ferrari, M. C.; Galizia, M.; De Angelis, M. G.; Sarti, G. C. *Ind. Eng. Chem. Res.* **2010**, *49*, 11920.
(22) Robeson, L. M. *J. Membr. Sci.* **1991**, *62*, 165.
(23) Robeson, L. M. *J. Membr. Sci.* **2008**, *320*, 390.
(24) Diaz, K.; Lopez-Gonzalez, M.; del Castillo, L. F.; Riande, E. *J. Membr. Sci.* **2011**, *383*, 206.
(25) Goh, P. S.; Ismail, A. F.; Sanip, S. M.; Ng, B. C.; Aziz, M. *Sep. Purif. Technol.* **2011**, *81*, 243.
(26) Noble, R. D. *J. Membr. Sci.* **2011**, *378*, 393.
(27) Aroon, M. A.; Ismail, A. F.; Matsuura, T.; Montazer-Rahmati, M. M. *Sep. Purif. Techol.* **2010**, *75*, 229.
(28) Adams, R.; Carson, C.; Ward, J.; Tannenbaum, R.; Koros, W. J. *Microporous Mesoporous Mater.* **2010**, *131*, 13.
(29) Ghosal, K.; Freeman, B. D. *Polym. Adv. Tech.* **1994**, *5*, 673.
(30) Raharjo, R. D.; Freeman, B. D.; Paul, D. R.; Sarti, G. C.; Sanders, E. S. *J. Membr. Sci.* **2007**, *306*, 75.
(31) Das, M.; Koros, W. J. *J. Membr. Sci.* **2010**, *365*, 399.
(32) Galizia, M. *Mass transport in polymeric and nanocomposite membranes for gas separation*, Ph.D. Thesis, University of Bologna, 2010 (in Italian).
(33) De Angelis, M. G.; Sarti, G. C.; Doghieri, F. *J. Membr. Sci.* **2007**, *289*, 106.
(34) Singh, A.; Freeman, B. D.; Pinnau, I. *J. Polym. Sci., B: Polym. Phys.* **1998**, *36*, 289.
(35) Barrer, R. M.; Barrie, J. A.; Slater, J. *J. Polym. Sci.* **1958**, *27*, 177.
(36) Sanders, E. S.; Koros, W. J.; Hopfenberg, H. B.; Stannett, V. *J. Membr. Sci.* **1984**, *18*, 59.
(37) Bondar, V. I.; Kamiya, Y.; Yampolskii, Y. *J. Polym. Sci., B: Polym. Phys.* **1996**, *34*, 369.
(38) Doghieri, F.; Sarti, G. C. *Macromolecules* **1996**, *29*, 7885.
(39) Sanchez, I. C.; Lacombe, R. H. *J. Phys. Chem.* **1976**, *80*, 2352.
(40) Sanchez, I. C.; Lacombe, R. H. *Macromolecules* **1978**, *11*, 1145.
(41) Sarti, G. C.; Doghieri, F. *Chem. Eng. Sci.* **1998**, *19*, 3435.
(42) Doghieri, F.; Sarti, G. C. *J. Membr. Sci.* **1998**, *147*, 73.
(43) De Angelis, M. G.; Merkel, T. C.; Bondar, V. I.; Freeman, B. D.; Doghieri, F.; Sarti, G. C. *J. Polym. Sci., B: Polym. Phys.* **1999**, *37*, 3011.
(44) Fleming, G. K.; Koros, W. J. *Macromolecules* **1990**, *23*, 1353.
(45) De Angelis, M. G.; Merkel, T. C.; Bondar, V. I.; Freeman, B. D.; Doghieri, F.; Sarti, G. C. *Macromolecules* **2002**, *35*, 1276.
(46) Giacinti Baschetti, M.; Doghieri, F.; Sarti, G. C. *Ind. Eng. Chem. Res.* **2001**, *40*, 3027.
(47) Guerra, G.; Manfredi, C.; Musto, P.; Tavone, S. *Macromolecules* **1998**, *31*, 1329.
(48) Albunia, A. R.; Musto, P.; Guerra, G. *Polymer* **2006**, *47*, 234.
(49) Crank, J. *The Mathematics of Diffusion*; Academic Press: New York, 1968.
(50) Zoller, P.; Fakhreddine, Y. A. *Thermochem. Acta* **1994**, *238*, 397.
(51) Pottinger, M. T.; Laurence, R. L. *J. Polym. Sci., Polym. Phys. Ed.* **1984**, *22*, 903.
(52) Hariharan, R.; Freeman, B. D.; Carbonell, R. G.; Sarti, G. C. *J. Appl. Polym. Sci.* **1993**, *50*, 1781.
(53) Perry, R. H.; Green, D. W. *Chemical Engineers' Handbook*, 7th ed.; McGraw-Hill: New York, 1999 (section 2).
(54) Mizumoto, T.; Masuda, T.; Higashimura, T. *J. Polym. Sci. A: Polym. Chem.* **1993**, *31*, 2555.
(55) Nagel, C.; Gunther-Schade, K.; Fritsch, D.; Strunskus, T.; Faupel, F. *Macromolecules* **2002**, *35*, 2071.
(56) Park, H. B.; Jung, C. H.; Lee, Y. M.; Hill, A. J.; Pas, S. J.; Mudie, S. T.; Van Wagner, E.; Freeman, B. D.; Cookson, D. J. *Science* **2007**, *318*, 254.
(57) Staudt-Bickel, C.; Koros, W. J. *J. Membr. Sci.* **2000**, *170*, 205.
(58) Tanaka, K.; Taguchi, A.; Hao, J.; Kita, H.; Okamoto, K. *J. Membr. Sci.* **1996**, *121*, 197.
(59) Giacinti Baschetti, M.; Ghisellini, M.; Quinzi, M.; Doghieri, F.; Stagnaro, P.; Costa, G.; Sarti, G. C. *J. Mol. Struct.* **2005**, *739*, 76.
(60) Okazaki, I.; Wunderlich, B. *J. Polym. Sci., Part B: Polym. Phys.* **1996**, *34*, 2941.
(61) Lin, J.; Shenogin, S.; Nazarenko, S. *Polymer* **2002**, *43*, 4733.